Shape Preservation Based on Gaussian Radial Basis Function Interpolation on Human Corpus Callosum

Umut Orcun Turgut(✉) and Didem Gokcay

Informatics Institute, METU, Ankara, Turkey
umut.turgut@gmail.com, didemgokcay@gmail.com

Abstract. The Corpus Callosum (CC) has been a structure of much interest in neuroimaging studies of normal brain development, schizophrenia, autism, bipolar and unipolar disorder. In this paper, we present a technique which allows us to develop a shape preservation methodology in the deformation of CC for further global and regional shape analyzes between two sample corpora callosa. Source and target CC are superpositioned individually from eleven anchor points. Source CC is deformed in order to get superpositioned onto the target CC from these anchor points and superposition operation leads other anatomical landmarks to get placed automatically in all of the regions of source CC for further deformation analysis. Region construction via quadratic Bézier curves, deformation by using Gaussian RBF and quantifying the amount of deformation via generalized Procrustes analysis are used to infer the proper parameters used in minimum deformation. Amount of deformation can be analyzed both regionally and globally.

Keywords: Shape preserving interpolation · Radial Basis Functions · Space deformation

1 Introduction

Investigating the regional differences between samples of Corpus Callosum (CC) is a widely observed task in morphological studies. The gold standard in these kinds of studies is the works performed by the anatomists. For instance an anatomist may only describe the slightly thinned splenium between two corpora callosa in the right manner by just checking the MRI data. Currently there is no such an anatomic system which can point out this kind of anatomical difference into a semantic description like the one anatomist performs.

Shape is a property that keeps its characteristics when rotated or translated. Scaling and shearing make the shape of objects alter. In order to perform a prosperous regional comparison between two corpora callosa, a superposition operation that will align the source CC onto the target CC is needed to be carried out. The superposition operation should be performed from the handle points that are pointing anatomically to the same location in both structures.

M. Reuter et al. (Eds.): SeSAMI 2016, LNCS 10126, pp. 118–132, 2016.
DOI: 10.1007/978-3-319-51237-2_10

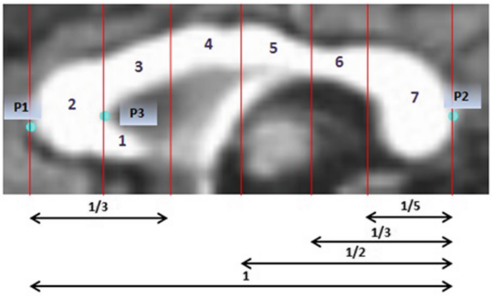

Fig. 1. Regional subdivision of the CC according to the study [15]. Parcellation landmarks are displayed as cyan circles. (Color figure online)

Those points are the key components of our mathematical model. For a near accurate comparison, shape deformation in this process must be minimal and the source structure should preserve its shape as much as possible after deformation.

In [15], author proposes an approach to define the regions of CC according to the anatomical connectivity. Figure 1 is showing the seven regional subdivisions, numbered 1 to 7, that will be also used in this study. P1 and P2 indicate the anteriormost and posteriormost points of the callosum with P1-P2 defined as the length of the callosum. Point P3 is the anteriormost point on the inner convexity of the anterior callosum. P1-P2 line is used as the linear axis to subdivide the callosum into anterior and posterior halves; anterior, middle, and posterior thirds; and the posterior one-fifth region (region 7). The line passing through P3, that is also perpendicular to the to the P1-P2 axis is used for defining the anteriormost division of the CC which generates regions rostrum (region 1) and genu (region 2). Region 3 is called as rostral body and it is the anteriormost one-third of the CC minus regions 1 and 2. Region 4 is called as anterior midbody and it is defined as the anterior one-half minus the anterior one-third. As for region 5, it is posterior midbody and is defined as the posterior one-half minus the posterior one-third. Region 6 is isthmus and it is defined as the posterior one-third minus the posterior one-fifth. Regions 3, 4, 5 and 6 constitute the body of the callosum. Regions, their anatomical labels and the callosal fibres in relation to cortical regions of origin and termination is displayed in Table 1.

The deformation function f basically maps the points p in the source CC to the new coordinates q; thus making the structure deformed. The deformation function needs to be built carefully and must hold the following properties [11]:

- Interpolation: The handle points p should map directly to q under deformation. (i.e. $f(p_i) = q_i$)
- Smoothness: f should produce smooth deformations
- Identity: If the deformed handles q are the same as p, then f should be the identity function. (i.e. $q_i = p_i \Rightarrow f(v) = v$)

These properties are similar to the ones that are used in the scattered data interpolation. In this paper, we introduce a deformation function that holds the

all requirements covered above. Source CC is superpositioned onto the target CC from some handle points under the mathematical model of Gaussian Radial Basis Function (RBF). A mathematical model which maps the handle points of the source CC to anatomically the same handle points of target CC is calculated. Apart from these handle points, the model also affects the rest of the points on the boundary of source CC; thus making a deformation on the source CC shape. Our aim in this study is proposing a robust method for nearly preserving the characteristics of source CC shape after by localizing the deformations instead of globally deforming the whole CC.

Table 1. CC regions displayed in Fig. 1 and their anatomical locations [15].

Region	Anatomical label	Cortical region
1	Rostrum	Caudal/orbital prefrontal, inferior premotor
2	Genu	Prefrontal
3	Rostral body	Premotor, supplementary motor
4	Anterior midbody	Motor
5	Posterior midbody	Somaesthetic, posterior parietal
6	Isthmus	Superior temporal, posterior parietal
7	Splenium	Occipital, inferior temporal

Contributions. We offer a non-linear space deformation technique which lacks a cage that has to be defined before the interactive deformation operations start. Eleven handle points scattered through the borders of seven regions in CC replaces the cage and these handle points are defined semi-automatically via our framework. Our technique offers a simple formulation and is specific to the input shape which calculates the right parameters for minimal deformation and surface detail preservation for further comparison operations. In addition, it can be extended to 3D neuroanatomical structure studies with the proper anatomical anchor points. Our method is robust and efficient.

This paper is organized as follows: In the next section we address the related works; in Sect. 3, we describe the mathematical model; Sect. 4 includes the functionalities that can be included to the study and lastly in Sect. 5 future work is presented.

2 Related Work

Shape manipulation studies are performed under two categories, namely space deformation methods and surface-based methods. In the space deformation methods, the space that holds the object is deformed and hereby deforms the shape. As for the other one, shape deformation is carried out by using the object solely.

Space deformation techniques are much simpler and require less computational cost than surface-based methods since the deformation is carried out on the space that surrounds the mesh of the object rather than the mesh itself. They have less control on the shape detail preservation. Surface-based methods; however, depend on the mesh that wraps up the object; therefore, mesh quality becomes an important factor in these kinds of studies. The main advantage of the surface-based methods is the detail preservation on the shape. Due to this property, systems of surface-based methods are computationally expensive.

Zohar Levi et al. [6] offered a space deformation framework for real-time shape deformation which does not have a major effect on the local shape and volume. The technique for deformation is controlled locally and does not have an influence on the nearby branches. It is based on Interior Radial Basis Functions (IRBF) and local distortions are minimized by minimizing the distortion of a set of spheres that are placed within the object. Another space deformation technique that is based on triharmonic radial basis functions for real-time freeform shape editing is proposed in the study of Botsch et al. [2]. In this study, the desired target shape is not exactly defined before the deformation process starts. The deformation is put into practice in an interactive manner.

Using a predefined skeleton and free-form deformation (FFD) are also the popular space-deformation methods that have been used in shape manipulation studies. In the former one, the user defines a skeleton to the shape and the system adjusts the shape relative to the skeleton [7]. It has some disadvantages on the objects which structurally do not have any skeleton such as jellies. A sequence of lattices which converge to a region in 3D is created in an FFD study [10]. Each point is associated with a lattice. As the points in the lattice are modified, a deformation of the space is created, and the embedded points are relocated within that deformed space.

A space deformation method that is called as cage-based Variational Harmonic Map (VHM) is suggested by Ben-Chen et al. [1]. In this technique, manual editing of the cage is replaced by controlling it with intuitive positional and rotational constraints that are enforced through energy minimization, which optimizes the deformation rigidity and smoothness. Sederberg et al. proposed a method that includes a control lattice for shape deformation [12]. Lattices are proved to be problematic for controlling the articulated objects.

Mean Value Coordinates (MVC), Harmonic Coordinates (HC) and Green Coordinates (GC) are three forms of cage-based space deformation methods. A cage is a polyhedron which has a similar shape to the enclosed object. The points inside the cage are represented by affine sums of the cage's vertices multiplied by special weight functions. Manipulation on the cage makes its interior get deformed smoothly. The work presented in the study [8] is a cage-based technique which builds upon the positive MVC. These coordinates are used for mesh deformation. A similar study that is replacing the MVC with HC is proposed in the study [5]. This replacement makes each cage vertex non-negative and falls off with distance as measured within the cage. GCs that are derived from Green functions introduce appropriate rotations into the space deformation in order to

allow shape preservation [9]. Weber et al. shows that GCs in the study [9] are a special case of complex barycentric coordinates and provides a simple analytic formula for them. Also an improvement on the GC is carried out and a new complex barycentric coordinates for 2D shape deformation is proposed in which the deformation better fits the user's specifications [14].

In the study of [13], the deformation is defined using a deformation graph which roughly conforms to the input shape. Deformation graphs are consisting of a varying number of nodes that the total size is related to the types of the edits that are going to take place. Coarse edits need fewer nodes than the detailed ones. An affine deformation is associated with each node in the deformation graph, which describes the transformation this node undergoes. The problem is stated as 'embedded deformation' since the algorithm must deform space through direct manipulation of objects within it, while preserving the embedded objects' features. Botsch et al. [3] puts forth a volumetric approach that is originated from the elastic energies of solid objects. The shape is break into voxels and the deformation is defined on them.

Igarishi et al. [4] proposes a point-based (surface-based) image deformation technique which results in a deformation that is called 'rigid-as-possible'. In this work, the amount of local scaling and shearing of deformations is minimized. The method is based on triangulation of the image and solving a linear system of equations whose size is equal to the number of vertices in the triangulation. In the study, the movement of vertices affects the positions of the other vertices in a way which results in a minimum distortion of each relevant triangle. Schaefer et al. [11] takes as a base of the study [4] and accelerates the deformations by solving a small linear system at each point in a uniform grid. This results in a very fast deformation of grids comprising tens of thousands of vertices in real time. Three classes of linear functions (affine, similarity and rigid) are used in the deformation method which is based on moving least squares.

Table 2. Points used in superposition operation and their anatomical locations.

Anchor point	Anatomical location
IP1	Intersection of regions rostrum & rostral body
IP2	Intersection of regions rostrum & genu
IP3	Intersection of regions genu & rostral body
IP4	Intersection of regions rostral body & anterior midbody (superior)
IP5	Intersection of regions anterior midbody & posterior midbody (superior)
IP6	Intersection of regions posterior midbody & isthmus (superior)
IP7	Intersection of regions isthmus & splenium (superior)
IP8	Intersection of regions isthmus & splenium (inferior)
IP9	Intersection of regions posterior midbody & isthmus (inferior)
IP10	Intersection of regions anterior midbody & posterior midbody (inferior)
IP11	Intersection of regions rostral body & anterior midbody (inferior)

The work presented here belongs to the space deformation category. Our main goal is to minimize the local deformations, thus to keep the localized characteristics of source CC regions, while superposing two corpora callosa for shape comparison. In this manner accurate semantic definition from the operation may be inferred. RBF is used for the deformation model where Gaussian is the basis function of the model. Eleven intersection points of seven callosal regions are defined as anchor points which are RBF centers at the same time. Anchor point decision affects the shape of deformation substantially. Decided points should be the same anatomical locations of corpora callosa for an efficient regional comparison. Apart from the number of total anchor points, the variance values of anchor points also affect the amount of deformation. Landmarks on the CC segments may be affected from just one anchor point or a combination of several anchor points. Proper variance values for each anchor point is one of the key studies of our work. These anchor points are summarized in Table 2 and displayed as orange circles in Fig. 2. Anchor points on the target CC are the final points that the initial ones will converge with the appropriate RBF weights. These weights are calculated according to the model. Proper weight value for each RBF center is decided after an iterative job which in the end lasts in a minimum localized source CC deformation. An error function is sum of squares of the difference between the actual source CC landmark coordinate before deformation and the one after deformation. The higher the function value, the more is the deformation. Therefore, error function searches for the proper weight values. General Procrustes Analysis (GPA) is used for calculating the morphological difference between two structures in this iterative job.

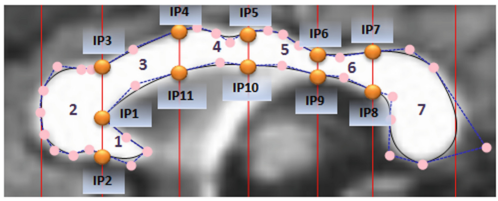

Fig. 2. Anchorage points for the superposition operation. (Color figure online)

Our method is basically as follows;

i. Source and target CC are parcellated into regions semi-automatically, in the guidance of the study [15].
ii. Manual shape modeling via quadratic Bézier curves is performed after regional parcellation.
iii. Source CC is superpositioned onto the target CC from the anchor points by the use of Gaussian RBF and a mathematical model is calculated.
iv. The parameters of the model are investigated with a method that is similar to Expectation Maximization (EM) for the minimum source CC deformation.

3 Shape Preservation with Gaussian RBF Interpolation

3.1 CC Parcellation

Samples of corpora callosa that are going to be investigated for regional differences are parcellated into compartments as an initial work. This process is performed semi-automatically in which three landmarks are needed to be manually defined on each CC image that has been loaded to the frame. The system then automatically divides the CC into seven regions as defined in the study [15]. Table 3 shows the points needed to parcellate the CC.

The boundaries of the callosal regions are calculated automatically with the positions of user defined landmarks and borders on the model are drawn. The whole operation lasts less than a minute for each CC. Figure 1 displays the segmented CC according to these parcellation landmarks. According to experimental work with monkeys and from postmortem studies of humans, a rough topography of callosal fibres in relation to cortical regions of origin and termination is displayed in Table 1.

3.2 CC Modeling

Quadratic Bézier curves are the building blocks of the modeling process. All of the callosal curves are represented with them.

A Bézier curve, specified by *n+1* control points, is a parametric curve segment of order *n*. It is defined according to a parameter t over the interval $0 \leq t \leq 1$ and is formally expressed according to the polynomial series;

$$B(t) = \sum_{i=0}^{n} b_i B_{i,n}(t) \tag{1}$$

where *b0, b1, . . . , bn* are the control points of the curve and;

$$B_{i,n}(t) = \begin{cases} \frac{n!}{(n-i)!i!}(1-t)^{n-i}t^i & 0 \leq i \leq n \\ 0 & otherwise \end{cases} \tag{2}$$

are the Bernstein polynomials.

A curve segment is defined manually by defining these control points on the interface. User basically clicks on the frame and when the count of control point number reaches three, a quadratic Bézier curve is automatically formed according to the Eq. 1 and drawn on the interface. A region may consist of several Bézier curves and all of the curves are continuously connected to the adjacent curve segments. There is no gap either locally in a region or between the two adjacent callosal regions. Fine tuning of the user drawn segments is performed by just moving the control points of the Bézier curve segment. All seven regions are constructed in an anterior-posterior axis starting from the Rostrum.

Modeling operation lasts longer than parcellation. Each region needs seperate modeling. Thus, whole operation may last up to 7–8 minutes for each CC.

Table 3. Parcellation landmarks of the CC.

User defined points	Anatomical definition
P1	Anteriormost point of the CC
P2	Posteriormost point of the CC
P3	Inner convexity of the anterior CC

This may be the major drawback of our method if a large data set is under study. For a more powerful method, the modeling operation should be performed automatically.

Regional construction of callosal curves on the CC which is shown on Fig. 1 is displayed in Fig. 3.

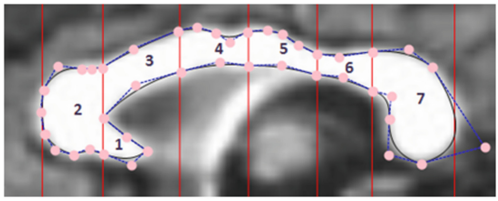

Fig. 3. Regional construction of callosal curves on the CC of Fig. 1. (Control polygons of each quadratic Bzier curve segment are displayed with blue dotted lines.) (Color figure online)

3.3 Regional Landmark Determination

Landmarks are determined in particular to the callosal regions. Total number of the landmarks is related with the total length of the curve segments in that region. The more the total length is the more the count of regional landmarks.

Separate curve which comprises of several quadratic Bézier curve segments is the key point in the determination of landmarks. Separate curves of a single region do not join; they are totally disjoint. The landmark determination and distribution is accomplished in particular to these separate curves. Since identical regions of two corpora callosa will have the same number of separate curves, one-to-one correspondence will be set between these curves and landmark operations are carried out particularly. This operation is performed for all of the separate curves of the region that is under study.

Figure 4 shows the landmark distribution in two callosal regions, namely rostrum and genu. There is one separate curve for each region and the length of this separate curve is used as a parameter in deciding the total number of landmarks. Figure 4 (a) shows callosal regions of Subject1 where red spots are indicating the positions of landmarks whereas (b) shows the callosal regions of Subject5. Here, in this example, it is seen that, 12 landmarks are calculated

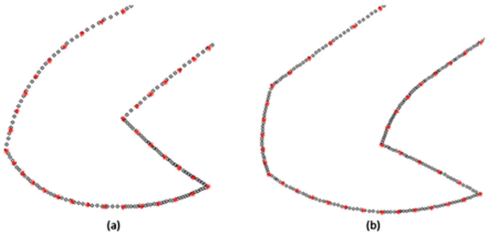

Fig. 4. Landmark distribution displayed in red on the segments of two callosal regions of **(a)** Subject1 **(b)** Subject5. (Color figure online)

for rostrum whereas 19 are for genu in both corpora callosa. There is one-to-one correspondence between these landmark pairs and all are used for further operations such as GPA.

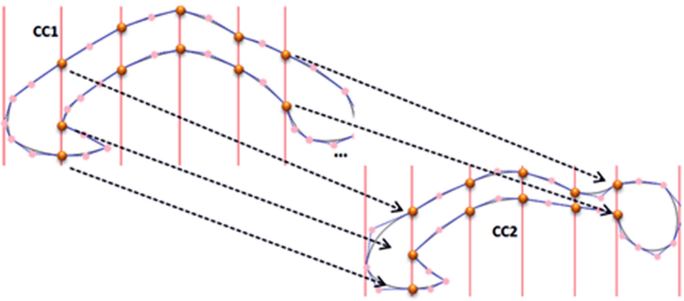

Fig. 5. One-to-one correspondence between the anchor points of two corpora callosa

3.4 Superposition

Superposition operation develops a mathematical model via the anchor points of source (CC1) and target (CC2) corpora callosa. This mathematical model is based on Gaussian RBF.

$$s(x) = a_0 + a_1 x + a_2 y + \sum_{i=1}^{N} \lambda i \phi(\|x - x_i\|) \tag{3}$$

where; $s(x)$ is the RBF, $\phi(r)$ is the basis function, $(r = \|x - x_i\|), \|x\|$ is the Euclidean norm, the λ_i's are the RBF weights and the x_i's are the RBF centers.

The RBF consists of a weighted sum of a radially symmetric basic function $\phi(r)$ located at the centers x_i and a low degree polynomial $a_0 + a_1 x + a_2 y$. Given a set of N points x_i and values f_i, the process of finding an interpolating RBF is called fitting, such that:

$$s(x_i) = f_i, i = 1, 2, ..., N \tag{4}$$

The fitted RBF is defined by the λ_i, the coefficients of the basic function in the summation, together with the coefficients of the polynomial term $a_0 + a_1 x + a_2 y$.

RBF has proven to be an effective tool in multivariate interpolation problems of scattered data. Here in this operation, anchor points lying on the curve segments are the key components of the basis functions. There is a one-to-one correspondence from all of the eleven anchor points of CC1 to the CC2 as displayed in Fig. 5.

Weight Vector Calculation: Equation 4 can be rewritten in matrix form as a linear system;

$$Hw = b \tag{5}$$

$$H = \begin{bmatrix} \phi(||x_1 - x_1||) & \phi(||x_1 - x_2||) & \dots & \phi(||x_1 - x_N||) & 1 & x_1 & y_1 \\ \phi(||x_2 - x_1||) & \phi(||x_2 - x_2||) & \dots & \phi(||x_2 - x_N||) & 1 & x_2 & y_2 \\ \vdots & \vdots & \dots & \vdots & \vdots & \vdots & \vdots \\ 1 & 1 & \dots & 1 & 0 & 0 & 0 \\ x_1 & x_2 & \dots & x_N & 0 & 0 & 0 \\ y_1 & y_2 & \dots & y_N & 0 & 0 & 0 \end{bmatrix}$$

$$w^T = (\lambda_1, \lambda_2, ..., \lambda_N, a_0, a_1, a_2)$$

$$b^T = (f_1, f_2, ..., f_N, 0, 0, 0)$$

where the dimension of interpolation matrix H is $(N+3, N+3)$, weight matrix w is $(N+3, 1)$ and the result matrix b is $(N+3, 1)$. Solving the linear system (Eq. 5) determines λ_i's and a's. The RBF that is used in this study is Gaussian, that is;

$$\phi(r) = e^{(-(\frac{1}{2\sigma^2})r^2)} \tag{6}$$

where σ is the standard deviation value of the relevant RBF center. In our model RBF centers (x_i) are the eleven anchor points of CC1 (N is 11) whereas b's are the coordinates of anchor points of CC2. Interpolation matrix (H) is formed by taking into account of the eleven anchor points of CC1. Row values are calculated in particular to an anchor point. For example first row includes the Gaussian RBF function values of all eleven anchor points according to anchor point IP1. The last three columns in the same row are filled with the values of 1, x and y coordinate values of IP1, respectively. Likewise second row includes the Gaussian RBF values according to anchor point IP2, and so on. First eleven columns of the last three rows in the interpolation matrix includes values of 1, x and y coordinate values of IP$ where $ is equal to the column number. The 3×3 submatrix in the lower right corner is the zero matrix. When nonsingular H matrix is prepared, weight matrices which are going to be used in superposition operation are calculated according to the equations;

$$w_x = H^{-1} b_x, w_y = H^{-1} b_y \tag{7}$$

Deciding the New Coordinates: Weight matrices which are calculated in the previous step are used in calculating the new coordinates of every single point that forms the Bézier curve segments of CC1. Interpolation matrix H is prepared by the use of point which is going to be deformed on the CC1 and the eleven anchor points, as in Eq. 5. The dimension of the H matrix will be $(1, N+3)$. While calculating the values of first eleven columns in the matrix H, standard deviation value of the relevant anchor point is used, as shown with $\sigma_\$$ symbol in Fig. 6.

(x, y) coordinate pair for all of the points on the Bézier curve segments of CC1 after deformation is calculated with the matrix multiplication of interpolation matrix H and w_x, interpolation matrix H and w_y, respectively.

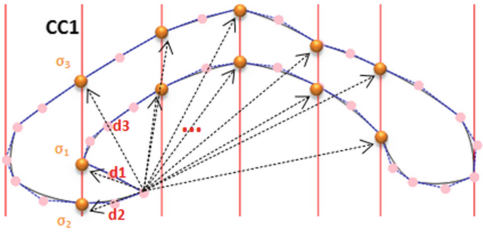

Fig. 6. Interpolation matrix (H) formation for calculating deformed coordinate pair.

Superposition Operation: The application of superposition operation requires basically determining anchor points and calculating mathematical model of the deformation.

The model that was prepared is applied to every points which form the regional curve segments. Carrying model into execution forms the deformed shape. Figure 7 shows **(a)** the source CC before deformation, **(b)** the target CC that the source is going to be superimposed on from the eleven anchor points, **(c)** the CC after deformation.

3.5 Minimum Deformation Calculation

The standard deviation value of each anchor points effects the outcome. Therefore, these values are treated as parameters to be learned. We run an iterative approach that is like the Expectation Maximization algorithm in mixture of Gaussians. This method makes us calculate different standard deviation values for each of the anchor points. As a result minimum deformation may be derived. Three step iterative approach is basically pointed out below.

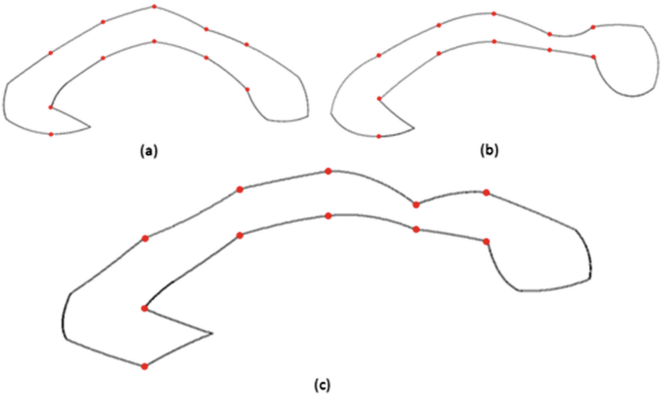

Fig. 7. Superposition operation. **(a)** CC before deformation **(b)** target CC to get anchored **(c)** CC after deformation via RBF model that is based on anchor points all of which have standard deviation values of 0.5 (red dots indicate the eleven anchor points). (Color figure online)

i. Fix all standard deviation (σ) values and solve for weight vectors.
ii. Fix weight vectors and minimize error function with respect to σ.
iii. With newly calculated σ values, solve for weight vectors again.
iv. Go to step i until maximum number of iterations is exceeded or difference of σ_i and σ_{i+1} are below a defined threshold value.

Our error function is the common sum-of-squares error, that is;

$$E(x) = \frac{1}{2}\sum_{k=1}^{c}(y_k(x) - t_k)^2 \tag{8}$$

The derivative of this error with respect to the standard deviation of basis function j, (σ_j), is;

$$\frac{\partial E}{\partial \sigma_j}(x) = \sum_{k}(y_k(x) - t_k)w_{kj}e^{\frac{\left\|(x-x_j)^2\right\|}{2\sigma_j^2}\frac{\left\|(x-x_j)^2\right\|}{\sigma_j^3}} \tag{9}$$

where c is the total number of landmarks on the CC boundary, $y_k(x)$ is the desired value and t_k is the actual value of that point.

$$\sigma_j = \sigma_j - n\frac{\partial E}{\partial \sigma_j} \tag{10}$$

where n is the learning rate.

4 Conclusion

37 source corpora callosa obtained from both normal subjects and subjects suffering from Major Depression Disorder (MDD) are studied according to the

model covered in this paper. Also an atlas CC is added as a target CC model to the study. The experiment is as follows;

i. Each source CC among 37 subjects is superimposed onto the target CC and proper parameters of all anchor points for the minimum deformation are obtained.
ii. 37 separate Procrustes distance value are calculated between the pairs of deformed source corpora callosa and target CC.
iii. The effect of deformation on the original source CCs is investigated via t-test whether it produces statistically significant results or not.

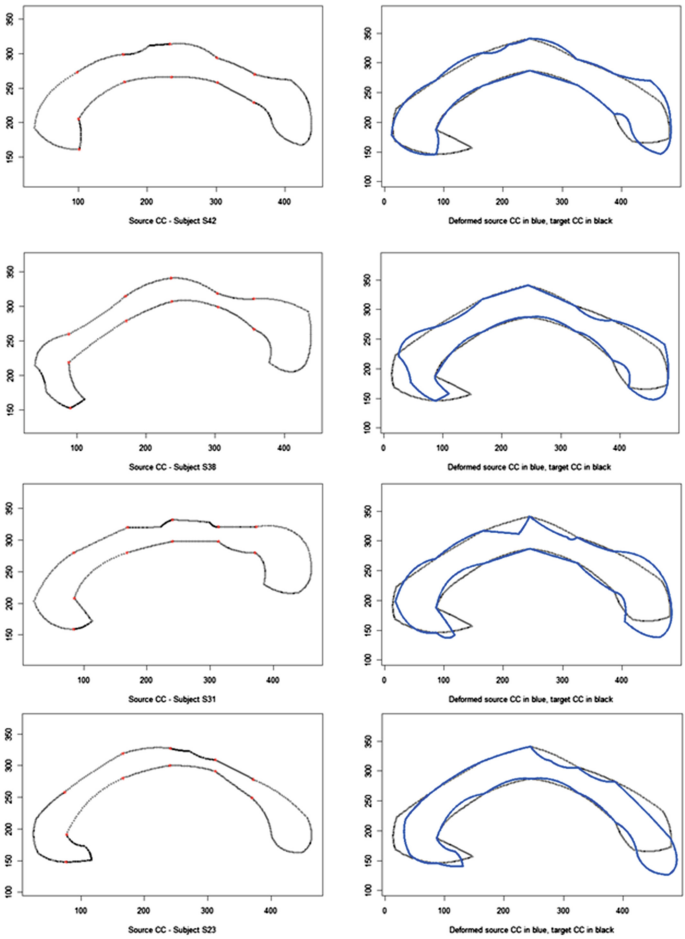

Fig. 8. Deformation operation. Source CC's are deformed according to the target CC via RBF that is holding proper parameters for each anchor points. (Color figure online)

Figure 8 shows sample deformations in our experiment. Each row belongs to a different subject and deformation is performed according to the same atlas. In the figure, CCs on the left show the original CCs of three subjects and CCs that are drawn with blue lines on the right show the deformed shapes of relevant CC. The black CCs on the right are the same target structure that is also called as atlas in the paper.

The null hypothesis (Ho) in our experiment basically assumes that deformation has no effect on the CC shapes whereas alternative hypothesis (Ha) claims that statistically significant difference occurs on the CC shape structures after deformation. Calculated t-value for the experiment becomes 15.86, which means Ho hypothesis is need to be rejected. As a conclusion, deformation changes the structures of source CCs significantly.

5 Discussion

Modeling the CC can be fully automated. This will outcome the automated parcellation; automated modeling of callosal regions which includes deciding on the number of segments that will form the callosal boundary, drawing Bézier curve segments and merging them.

Some preprocessing steps before the selection of anchor points may also be included into the study.

6 Future Work

The same experiment is going to be performed with the methods of affine Moving Least Squares (MLS), similarity MLS, rigid MLS, GC, MVC, HC and rigid-as-possible. The inner-distance values such as Floyd-Warshall or Johnson instead of Euclidean distance may also be applied in the relevant models and the results are going to be compared with the one that is obtained in our study.

References

1. Ben-Chen, M., Weber, O., Gotsman, C.: Variational harmonic maps for space deformation. ACM Trans. Graph. (TOG) **28**, 34 (2009)
2. Botsch, M., Kobbelt, L.: Real-time shape editing using radial basis functions. In: Computer Graphics Forum, vol. 24, pp. 611–621. Wiley Online Library (2005)
3. Botsch, M., Pauly, M., Wicke, M., Gross, M.: Adaptive space deformations based on rigid cells. In: Computer Graphics Forum, vol. 26, pp. 339–347. Wiley Online Library (2007)
4. Igarashi, T., Moscovich, T., Hughes, J.F.: As-rigid-as-possible shape manipulation. ACM Trans. Graph. (TOG) **24**, 1134–1141 (2005)
5. Joshi, P., Meyer, M., DeRose, T., Green, B., Sanocki, T.: Harmonic coordinates for character articulation. ACM Trans. Graph. (TOG) **26**, 71 (2007)
6. Levi, Z., Levin, D.: Shape deformation via interior RBF. IEEE Trans. Vis. Comput. Graph. **20**(7), 1062–1075 (2014)

7. Lewis, J.P., Cordner, M., Fong, N.: Pose space deformation: a unified approach to shape interpolation and skeleton-driven deformation. In: Proceedings of the 27th Annual Conference on Computer Graphics and Interactive Techniques, pp. 165–172. ACM Press/Addison-Wesley Publishing Co. (2000)
8. Lipman, Y., Kopf, J., Cohen-Or, D., Levin, D.: GPU-assisted positive mean value coordinates for mesh deformations. In: Symposium on Geometry Processing (2007)
9. Lipman, Y., Levin, D., Cohen-Or, D.: Green coordinates. ACM Trans. Graph. (TOG) **27**, 78 (2008)
10. MacCracken, R., Joy, K.I.: Free-form deformations with lattices of arbitrary topology. In: Proceedings of the 23rd Annual Conference on Computer Graphics and Interactive Techniques, pp. 181–188. ACM (1996)
11. Schaefer, S., McPhail, T., Warren, J.: Image deformation using moving least squares. ACM Trans. Graph. (TOG) **25**, 533–540 (2006)
12. Sederberg, T.W., Parry, S.R.: Free-form deformation of solid geometric models. ACM SIGGRAPH Comput. Graph. **20**(4), 151–160 (1986)
13. Sumner, R.W., Schmid, J., Pauly, M.: Embedded deformation for shape manipulation. ACM Trans. Graph. (TOG) **26**, 80 (2007)
14. Weber, O., Ben-Chen, M., Gotsman, C.: Complex barycentric coordinates with applications to planar shape deformation. In: Computer Graphics Forum, vol. 28, pp. 587–597. Wiley Online Library (2009)
15. Witelson, S.F.: Hand and sex differences in the isthmus and genu of the human corpus callosum. Brain **112**(3), 799–835 (1989)